Inorganic Chemistry

Article

Copper(II) Hexaaza Macrocyclic Binuclear Complexes Obtained from the Reaction of Their Copper(I) Derivates and Molecular Dioxygen

Miquel Costas,[*,#] **Xavi Ribas,**[#] **Albert Poater,**[†] **Josep Maria López Valbuena,**[#] **Raül Xifra,**[#]
Anna Company,[#] **Miquel Duran,**[†] **and Miquel Solà**[*,†]

Departament de Química and Institut de Química Computacional, Universitat de Girona,
Campus de Montilivi, E-17071 Girona, Spain

Antoni Llobet*

Departament de Química, Universitat Autònoma de Barcelona, Bellaterra, 08193 Barcelona, Spain

Montserrat Corbella

Departament de Química Inorgànica, Universitat de Barcelona, Martí i Franquès 1−11, E-08028 Barcelona, Spain

Miguel Angel Usón

Departamento de Química Inorgánica, Instituto de Ciencia de Materiales de Aragón, Universidad
de Zaragoza, CSIC, E-50009 Zaragoza, Spain

José Mahía

Servicios Xerais de Apoio Á Investigación, Universidade da Coruña, E-15071 A Coruña, Spain

Xavier Solans

Departament de Cristal·lografia, Mineralogia i Dipòsits Minerals, Universitat de Barcelona,
Martí i Franquès s/n, E-08028 Barcelona, Spain

Xiaopeng Shan

Department of Chemistry, University of Minnesota, 207 Pleasant Street SE, Minneapolis, Minnesota 55455

Jordi Benet-Buchholz

Institut Català d'Investigació Química (ICIQ), Campus Universitari, Avinguda Països Catalans
s/n, E-43007 Tarragona, Spain

Density functional theory (DFT) calculations have been carried out for a series of Cu^I complexes bearing N-hexadentate macrocyclic dinucleating ligands and for their corresponding peroxo species (**1c**–**8c**) generated by their interaction with molecular O$_2$. For complexes **1c**–**7c**, it has been found that the side-on peroxodicopper(II) is the favored structure with regard to the bis(μ-oxo)-dicopper(III). For those complexes, the singlet state has also been shown to be more stable than the triplet state. In the case of **8c**, the most favored structure is the *trans*-1,2-peroxodicopper(II) because of the para substitution and the steric encumbrance produced by the methylation of the N atoms. Cu^{II} complexes **4e**, **5e**, and **8e** have been obtained by O$_2$ oxidation of their corresponding Cu^I complexes and structurally and magnetically characterized. X-ray single-crystal structures for those complexes have been solved, and they show three completely different types of Cu$^{II}_2$ structures: (a) For **4e**, the Cu^{II} centers are bridged by a phenolate group and an external hydroxide ligand. The phenolate group is generated from the evolution of **4c** via intramolecular arene hydroxylation. (b) For **5e**, the two Cu^{II} centers are bridged by two hydroxide ligands. (c) For the **8e** case, the Cu^{II} centers are ligated to terminally bound hydroxide ligands, rare because of its tendency to bridge. The evolution of complexes **1c**–**8c** toward their oxidized species has also been rationalized by DFT calculations based mainly on their structure and electrophilicity. The structural diversity of the oxidized species is also responsible for a variety of magnetic behavior: (a) strong antiferromagnetic (AF) coupling with $J = -482.0$ cm^{-1} ($g = 2.30$; $\rho = 0.032$; $R = 5.6 \times 10^{-3}$) for **4e**; (b) AF coupling with $J = -286.3$ cm^{-1} ($g = 2.07$; $\rho = 0.064$; $R = 2.6 \times 10^{-3}$) for **5e**; (c) an uncoupled Cu$^{II}_2$ complex for **8e**.

Introduction

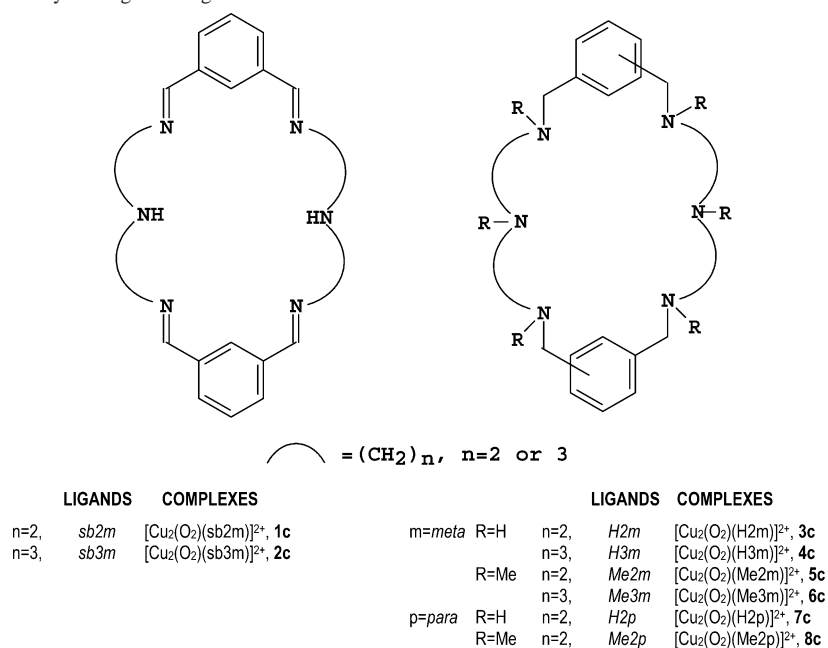Polynuclear complexes have been intensively investigated in fields that range from studies of their physical properties, with special attention to magnetic interactions,[1–4] to unique chemical reactivity patterns.[5–8] In both cases, the relative disposition of the metal centers and the bridging ligands are

---

* To whom correspondence should be addressed. E-mail: miquel.costas@udg.es (M.C.), miquel.sola@udg.es (M.S.), antoni.llobet@uab.es (A.L.).

\# Departament de Química.
† Departament de Química and Institut de Química Computacional.

Chart 1. Drawing of the Macrocyclic Ligands Together with the Abbreviations Used

= $(CH_2)_n$, n=2 or 3

LIGANDS		COMPLEXES
n=2,	sb2m	$[Cu_2(O_2)(sb2m)]^{2+}$, **1c**
n=3,	sb3m	$[Cu_2(O_2)(sb3m)]^{2+}$, **2c**

		LIGANDS		COMPLEXES
m=meta	R=H	n=2,	H2m	$[Cu_2(O_2)(H2m)]^{2+}$, **3c**
		n=3,	H3m	$[Cu_2(O_2)(H3m)]^{2+}$, **4c**
	R=Me	n=2,	Me2m	$[Cu_2(O_2)(Me2m)]^{2+}$, **5c**
		n=3,	Me3m	$[Cu_2(O_2)(Me3m)]^{2+}$, **6c**
p=para	R=H	n=2,	H2p	$[Cu_2(O_2)(H2p)]^{2+}$, **7c**
	R=Me	n=2,	Me2p	$[Cu_2(O_2)(Me2p)]^{2+}$, **8c**

key issues that determine their physical and chemical behavior.

A first approach toward the understanding and mastering of metal cooperation in chemical reactions involves the use of simple binuclear metal complexes. A recent work by Bosnich et al. elegantly shows how a substrate bound to a single metal center can be reduced using the reducing power of multiple metals.[8]

Nature also benefits from metal cooperation in a number of metalloproteins whose functions range from small-molecule activation (N_2, O_2, and H_2)[9-13] to hydrolysis.[14] Iron and copper metalloproteins containing a binuclear active site and implicated in the activation of molecular O_2 are of special interest. This is the case of hemocyanin and tyrosinase, which possess very similar active sites consisting of a binuclear Cu complex, although they have a completely different biological role.[12,15-17]

Low-molecular-weight models have been of great help to the understanding of the spectroscopic and structural properties of the active site of these proteins. From a reactivity point of view, model compounds have shown that subtle variations in the ligand design strongly affect their reactivity toward O_2 and the reactivity of the corresponding oxygenated complexes toward intramolecular oxidation or the oxidation of an external substrate.[18-21]

Modeling of the active site of binuclear O_2 processing metalloproteins (like tyrosinase or hemocyanin) has been carried out by mononuclear complexes that upon reaction with O_2 form binuclear complexes or by binuclear complexes containing a dinucleating ligand. The latter strategy allows the prearrangement of two metal centers with a particular M···M distance.[18-21]

Recently, we have shown that the family of dinucleating hexaaza macrocyclic ligands containing tertiary amines depicted in Chart 1 allows exertion of a certain control of the metal center local geometry as well as their relative disposition.[22,23] The present paper reports how the subtle variations exemplified in this family of ligands strongly influence the reactivity of their corresponding Cu^I_2 complexes toward molecular O_2 and their oxidative evolution. Previous studies by Menif and Martell and Schindler et al. have already addressed the O_2 chemistry of Cu_2 complexes containing the sb2m and sb3m ligand macrocycles,[24,25]

(1) Kahn, O. *Molecular Magnetism*; Wiley-VCH: New York, 1993.
(2) Carlin, R. L. *Magnetochemistry*; Springer-Verlag: Berlin, 1986.
(3) Kahn, O. In *Modular Chemistry*; Michl, J., Ed.; Kluwer Academic: Dordrecht, The Netherlands, 1997; Vol. 499, pp 287−302.
(4) Cornia, A.; Gatteschi, D.; Sessoli, R. *Coord. Chem. Rev.* **2001**, *219*, 573−604.
(5) Suzuki, M.; Furutachi, H.; Okawa, H. *Coord. Chem. Rev.* **2000**, *200−202*, 105−129.
(6) Gavrilova, A. L.; Bosnich, B. *Chem. Rev.* **2004**, *104*, 349−384.
(7) Gavrilova, A. L.; Qin, C. J.; Sommer, R. D.; Rheingold, A. L.; Bosnich, B. *J. Am. Chem. Soc.* **2002**, *124*, 1714−1722.
(8) Incarvito, C.; Rheingold, A. L.; Gavrilova, A. L.; Qin, C. J.; Bosnich, B. *Inorg. Chem.* **2001**, *40*, 4101−4108.
(9) Howard, J. B.; Rees, D. C. *Chem. Rev.* **1996**, *7*, 2965−2982.
(10) Wallar, B. J.; Lipscomb, J. D. *Chem. Rev.* **1996**, *96*, 2625−2658.
(11) Thauer, R. K.; Klein, A. R.; Hartmann, G. C. *Chem. Rev.* **1996**, *7*, 3031−3042.
(12) Solomon, E. I.; Chen, P.; Metz, M.; Lee, S.-K.; Palmer, A. E. *Angew. Chem., Int. Ed.* **2001**, *40*, 4570−4590.
(13) Belle, C.; Pierre, J.-L. *Eur. J. Inorg. Chem.* **2003**, 4137−4146.
(14) Wilcox, D. E. *Chem. Rev.* **1996**, *96*, 2435−2458.
(15) Kitajima, N.; Moro-oka, Y. *Chem. Rev.* **1994**, *94*, 737−757.
(16) Magnus, K. A.; Ton-That, H.; Carpenter, J. E. *Chem. Rev.* **1994**, *94*, 727−735.
(17) Solomon, E. I.; Sundaram, U. M.; Machonkin, T. E. *Chem. Rev.* **1996**, *96*, 2563−2605.

(18) Mirica, L. M.; Ottenwaelder, X.; Stack, T. D. P. *Chem. Rev.* **2004**, *114*, 1013−1046.
(19) Lewis, E. A.; Tolman, W. B. *Chem. Rev.* **2004**, *114*, 1047−1076.
(20) Kopf, M.-A.; Karlin, K. D. In *Biomimetic Oxidations Catalyzed by Transition Metal Complexes*; Meunier, B., Ed.; Imperial College Press: London, 2000; pp 309−362.
(21) Schindler, S. *Eur. J. Inorg. Chem.* **2000**, 2311−2326.
(22) Costas, M.; Xifra, R.; Llobet, A.; Solà, M.; Robles, J.; Parella, T.; Stoeckli-Evans, H.; Neuburger, M. *Inorg. Chem.* **2003**, *42*, 4456−4468.
(23) Costas, M.; Anda, C.; Llobet, A.; Parella, T.; Stoeckli-Evans, H.; Pinilla, E. *Eur. J. Inorg. Chem.* **2004**, *4*, 857−865.

demonstrating that ligand hydroxylation only occurs for the former.

Experimental Section

Materials and Synthesis. Solvents were purchased from SDS as reagent grade. Acetonitrile was distilled over P_2O_5 and stored over molecular sieves. Diethyl ether and tetrahydrofuran were distilled over sodium benzophenone under a N_2 atmosphere. Acetone was dried over $CaCl_2$ and stored over molecular sieves. Unless noted otherwise, all reagents were purchased from commercial sources and used as received. The preparation and handling of air-sensitive materials were carried out under an Ar or N_2 atmosphere using standard Schlenk techniques.

3,6,9,16,19,22-Hexamethyl-3,6,9,16,19,22-hexaazatricyclo-[22.2.2.2^{11,14}]triaconta-1(26),11(12),13,24,27,29-hexaene (Me2p), 3,6,9,17,20,23-hexamethyl-3,6,9,17,20,23-hexaazatricyclo[23.3.1.1^{11,15}]-triaconta-1(29),11(30),12,14,25,27-hexaene (Me2m), and 3,7,11,-19,23,27-hexaazatricyclo[27.3.1.1^{13,17}]tetratriaconta-1(32),13,15,-17(34),29(33),30-hexaene (H3m),[22,26] Cu(CH$_3$CN)$_4$X, where X = ClO$_4$ and PF$_6$,[27] [Cu$^I_2$(Me2p)(CO)$_2$](ClO$_4$)$_2$,[22] and [Cu$^I_2$(H3m)(CO)$_2$]-(PF$_6$)$_2$[28] were prepared according to the published procedures or with slight modifications thereof.

Caution! Perchlorate salts are potentially explosive and should be handled with care!

[Cu$^{II}_2$(H3m-O)(μ-OH)](PF$_6$)$_2$·0.5CH$_3$CN, 4e(PF$_6$)$_2$·0.5CH$_3$CN. [Cu$^I_2$(CO)$_2$(H3m)](PF$_6$)$_2$ (15 mg, 0.016 mmol) was charged in a Schlenk flask under a N_2 atmosphere and dissolved in a previously deoxygenated mixture of acetone/water (98:2, v/v; 3.4 mL). O$_2$ was bubbled through the solution for 5 min, turning the initial colorless solution to green. The solution was then filtered and left standing for 12 h, at which time CH$_3$CN (1 mL) was added. The mixture was filtered, and ether was slowly diffused to this solution to afford the product as green blocks (11 mg, 74%). FT-IR (KBr): ν 3444 (OH), 3296 (NH), 1459 (C=C arom), 844 and 558 (PF$_6$) cm^{-1}. Elem anal. Calcd (%) for Cu$_2$C$_{28}$H$_{46}$N$_6$O$_2$P$_2$F$_{12}$·0.5CH$_3$CN (936.25): C, 37.20; N, 9.72; H, 5.11. Found: C, 37.13; N, 9.77; H, 5.21. UV−vis (CH$_3$CN): λ_{max} (ϵ, dm^3·mol^{-1}·cm^{-1}) 342 (3490), 636 (406).

H3m-OH. 4e(PF$_6$)$_2$·0.5CH$_3$CN (16 mg, 0.017 mmol) was treated with aqueous ammonia/CH$_2$Cl$_2$ (1:1, v/v; 5 mL). The organic phase was separated and the water phase further extracted with CH$_2$Cl$_2$ (2 × 5 mL). The combined organic phases were dried over MgSO$_4$, filtered, and dried under vacuum to obtain H3m-OH (7.6 mg, 88%). ^{1}H NMR (200 MHz, CDCl$_3$, 25 °C): δ 7.24 (m, 4H), 6.98(d, 2H), 6.71 (t, 1H), 3.84 (s, 4H), 3.74 (s, 4H), 2.69 (m, 16H), 1.68 ppm (m, 8H). ^{13}C NMR (200 MHz, CDCl$_3$, 25 °C): δ 140.5, 128.8, 127.5, 126.8, 118.5, 53.9, 51.1, 48.6, 48.0, 29.7 ppm.

[Cu$^{II}_2$(μ-OH)$_2$(Me2m)](ClO$_4$)$_2$·CH$_3$CN, 5e(ClO$_4$)$_2$·CH$_3$CN. Me2m (50 mg, 0.10 mmol) and Cu(CH$_3$CN)$_4$ClO$_4$ (66 mg, 0.20 mmol) were charged in a Schlenk flask under a N_2 atmosphere and dissolved in previously deoxygenated CH$_3$CN/CH$_3$OH (1:1, v/v; 5 mL). The mixture was stirred for 5 min, and then CO was gently bubbled through for 5 min. At this time, the solution was exposed to air and left standing for 1 week, precipitating a blue-green solid. The solvent was decanted, and the precipitate was

recrystallized by slow diffusion of ether to a CH$_3$CN solution to afford the product as large blue-green blocks (46 mg, 51%). FT-IR (KBr, cm^{-1}): ν 3543 (OH), 1462 (C=C arom), 1091 and 620 (ClO$_4$) cm^{-1}. Elem anal. Calcd (%) for C$_{30}$H$_{51}$N$_6$Cu$_2$O$_9$Cl$_2$·CH$_3$-CN (895.82): C, 42.90; N, 10.94; H, 6.19. Found: C, 43.07; N, 11.05; H, 6.16. UV−vis (CH$_3$CN): λ_{max} (ϵ, dm^3·mol^{-1}·cm^{-1}) 274 (6850), 346 (2800), 624 (230). Crystals of **5e(ClO$_4$)$_2$·2CH$_3$OH** suitable for X-ray analysis were grown by slow ether diffusion to a CH$_3$CN/CH$_3$OH solution.

[Cu$^{II}_2$(μ-OH)$_2$(Me2m)](CF$_3$SO$_3$)$_2$·CH$_3$CN, 5e(CF$_3$SO$_3$)$_2$·CH$_3$CN. Method 1. Me2m (83 mg, 0.17 mmol) and [Cu(CH$_3$CN)$_4$]CF$_3$SO$_3$ (128 mg, 0.34 mmol) were charged in a Schlenk flask under a N_2 atmosphere and dissolved in previously deoxygenated CH$_3$CN/CH$_3$-OH (1:1, v/v; 5 mL). The mixture was stirred for 5 min, and then CO was gently bubbled through for 5 min. At this time, the solution was exposed to air and left standing for 1 week, becoming blue-green. Afterward, the solvent was removed under vacuum and the residue taken in CH$_3$CN (3 mL) and filtered through Celite. Vapor diffusion of ether caused precipitation of the product as a blue-green microcrystalline solid. The solvent was decanted and the precipitate was recrystallized by slow diffusion of ether to a CH$_3$-CN solution to afford the product as large blue-green blocks (45 mg, 28%).

Method 2. Me2m (100 mg, 0.20 mmol) and Cu(CF$_3$SO$_3$)$_2$ (149 mg, 0.40 mmol) were charged in a 10-mL flask and dissolved in CH$_3$CN (5 mL) to form a blue solution. The mixture was stirred for 30 min, and then a solution of NaOH (16 mg, 0.40 mmol) in water (0.5 mL) was added dropwise over 5 min while keeping the CH$_3$CN solution under vigorous agitation. The blue solution was stirred for 4 h and then filtered through Celite. Ether diffusion over this solution affords large blue blocks. The solvent was decanted and the crystalline solid dried under vacuum (98 mg, 49%). IR (KBr): ν 3543 (OH), 1462 (C=C arom), 1254, 1151, 1030 and 635 (CF$_3$SO$_3$) cm^{-1}. Elem anal. Calcd (%) for C$_{32}$H$_{52}$N$_6$-Cu$_2$O$_8$F$_6$S$_2$·CH$_3$CN (M_m = 995.06): C, 41.04; N, 9.85; H, 5.57; S, 6.45. Found: C, 40.68; N, 9.78; H, 5.76; S, 6.08. UV−vis (CH$_3$-CN): λ_{max} (ϵ, dm^3·mol^{-1}·cm^{-1}) 274 (6850), 346 (2800), 624 (230).

[Cu$^{II}_2$(OH)$_2$(Me2p)](CF$_3$SO$_3$)$_2$·2.5H$_2$O, 8e(CF$_3$SO$_3$)$_2$·2.5H$_2$O. Method 1. Me2p (83 mg, 0.17 mmols) and [Cu(CH$_3$CN)$_4$]CF$_3$SO$_3$ (128 mg, 0.34 mmol) were charged in a Schlenk flask under a N_2 atmosphere and dissolved in previously deoxygenated CH$_3$CN/CH$_3$-OH (1:1, v/v; 5 mL). The mixture was stirred for 5 min, and then CO was gently bubbled through for 5 min. At this time, the solution was exposed to air and left standing for 1 week, becoming blue. Afterward, the solvent was removed under vacuum and the residue taken in CH$_3$CN (3 mL) and filtered through Celite. Vapor diffusion of ether caused precipitation of a purple-blue microcrystalline solid. The solvent was decanted and the precipitate dried under vacuum (25 mg, 16%).

Method 2. Me2p (100 mg, 0.20 mmol) and Cu(CF$_3$SO$_3$)$_2$ (145 mg, 0.39 mmol) were charged in a 10-mL flask and dissolved in CH$_3$CN (5 mL) to form a reddish-blue solution. The mixture was stirred for 30 min, and then a solution of NaOH (16 mg, 0.40 mmol) in water (0.5 mL) was added dropwise over 5 min while keeping the CH$_3$CN solution under vigorous agitation. The resulting blue-purple solution was stirred for 4 h and then filtered through Celite. Ether diffusion over this solution affords after 2 days large blue-purple needles. The solvent was decanted and the crystalline solid dried under vacuum (158 mg, 84%). IR (KBr): ν 3586 (OH), 1474 (C=C arom), 1259, 1145, 1030 and 634 (CF$_3$SO$_3$) cm^{-1}. Elem anal. Calcd (%) for C$_{32}$H$_{52}$N$_6$Cu$_2$O$_8$F$_6$S$_2$·2.5H$_2$O (999.05): C, 38.47; N, 8.41; H, 5.75; S, 6.42. Found: C, 38.56; N, 8.10; H, 5.59; S, 6.27.

(24) Menif, R.; Martell, A. E. *J. Chem. Soc., Chem. Commun.* **1989**, *20*, 1521−1523.
(25) Utz, D.; Heinemann, F. W.; Hampel, F.; Richens, D. T.; Schindler, S. *Inorg. Chem.* **2003**, *42*, 1430−1436.
(26) Llobet, A.; Reibenspies, J.; Martell, A. E. *Inorg. Chem.* **1994**, *33*, 5946−5951.
(27) Kubas, G. J. *Inorg. Synth.* **1979**, *19*, 90−92.
(28) Ribas, X. Ph.D. Thesis, Universitat de Girona, Girona, Spain, 2001.

UV–vis (CH_3CN): λ_{max} (ϵ, dm³·mol⁻¹·cm⁻¹) 290 (11150), 495 (230), 636 (220).

Physical Methods. IR spectra were taken in a Mattson-Galaxy Satellite FT-IR spectrophotometer as solid KBr pellets. Elemental analyses were conducted in a Carlo Erba Instrument model CHNS 1108. UV–vis spectra were recorded on a HP-89532A UV–vis diode array spectrophotometer using quartz cuvettes. Variable-temperature magnetic susceptibility measurements were carried out in the polycrystalline state on a Faraday-type magnetometer (MANIC DSM8) equipped with a Bruker BE15 electromagnet and an Oxford CF 1200S cryogenic apparatus. Data were taken in the temperature range 4–300 K with an applied magnetic field of 15 000 G. Diamagnetic corrections were estimated from Pascal tables. Electron paramagnetic resonance (EPR) spectra were recorded on a Bruker EPP 300 spectrometer equipped with an Oxford ESR 910 liquid-helium cryostat and an Oxford temperature controller. For the fits, the agreement factor is defined as $R = \Sigma(\chi T_{cal} - \chi T_{exp})^2/\Sigma(\chi T_{exp})^2$.

Crystallographic Studies. Single-crystal X-ray analyses were performed on a Siemens CCD diffractometer [$4e(PF_6)_2$·0.5MeCN], a Bruker SMART CCD [$5e(ClO_4)_2$·2MeOH], and a Bruker SMART Apex CCD [$8e(CF_3SO_3)_2$·5H₂O] using λ(Mo Kα) radiation ($\lambda = 0.710\,73$ Å). The data collection was executed using the *SMART* program. Absorption corrections were carried out using *SADABS*. Cell refinements and data reduction were made by the *SAINT* program. The structures were determined by direct methods using the *SHELXTL* program and refined using full-matrix least squares. All non-H atoms were refined anisotropically, whereas the H atoms were placed at the calculated positions and included in the final stage of refinements with fixed thermal and positional parameters. The crystallographic refinement parameters for complexes **4e**·MeCN, **5e**·2MeOH, and **8e**·5H₂O are summarized in Table 4, and the selected bond distances and angles are listed in Table 5.

Computational Details. The reported calculations were carried out by using the Amsterdam density functional (ADF) package developed by Baerends et al.[29–31] and vectorized by Ravenek et al.[32] The numerical integration scheme employed was that of te Velde and Baerends.[33] An uncontracted triple-ζ basis set was used for describing the 3s, 3p, 3d, 4s, and 4p orbitals of Cu. For C (2s, 2p), N (2s, 2p), O (2s, 2p), and H (1s), double-ζ basis sets were employed. All of these basis sets were augmented by an extra polarization function.[34,35] Electrons in lower shells were treated within the frozen-core approximation.[29–31] A set of auxiliary s, p, d, f, and g functions, centered in all nuclei, were introduced in order to fit the molecular density and coulombic potential accurately in each self-consistent-field cycle.[36] Closed- and open-shell systems were studied within the restricted and unrestricted formalism,

respectively. Geometries were fully optimized within the local density approximation (LDA), which includes the X_α exchange ($\alpha = {}^2/_3$),[37] together with the electron gas correlation functional in the Vosko–Wilk–Nusair (VWN) parametrization.[38] The analytical gradients implemented by Versluis and Ziegler[39] were employed to perform geometry optimizations. Energies were evaluated at the LDA molecular geometries using a generalized gradient approximation (GGA) that includes a GGA exchange correction of Becke[40] and the GGA correlation correction of Perdew.[41] This method is labeled throughout this work as BP86//VWN. The 2000.02 release of the ADF package was used for all calculations.[42]

To analyze the electrophilicity of the optimized complexes, we have calculated the electrophilicity index defined by Parr et al. as[43]

$$\omega = \mu^2/2\eta \tag{1}$$

where μ and η are the chemical potential and molecular hardness, respectively. In the framework of the conceptual density functional theory (DFT),[44] the chemical potential and molecular hardness for an N-electron system with total electronic energy E and external potential $\nu(\vec{r})$ are defined as the first and second derivatives of the energy with respect to N at a fixed external potential $\nu(\vec{r})$.[45–47] In numerical applications, μ and η are calculated through the following approximate versions based upon the finite-difference approximation and Koopmans' theorem,[48]

$$\mu \cong \frac{1}{2}(\epsilon_L + \epsilon_H) \tag{2}$$

$$\eta \cong \frac{1}{2}(\epsilon_L - \epsilon_H) \tag{3}$$

where ϵ_H and ϵ_L are the energies of the highest occupied molecular orbital (HOMO) and the lowest unoccupied molecular orbital (LUMO), respectively.

To analyze the origin of the binding energy (BE) between the ground state of molecular O_2 and the binuclear macrocycle to form the μ-η^2: η^2-peroxo compounds, we have decomposed the BE into deformation and interaction energies. The deformation energy (ΔE_{def}) is the energy needed to modify the geometry of the ground-state free fragments to attain the geometry that they have in the intermediate species. It can be divided into the deformation energy of the binuclear complex ($\Delta E_{def\,complex}$) and the deformation energy of the O_2 molecule ($\Delta E_{def\,O_2}$). On the other hand, the interaction energy (ΔE_{int}) is the energy released when the two free deformed fragments in their ground states are brought to the position that they have in the intermediate species. Details on the starting structures for geometry optimization can be found in the Supporting Information.

(29) Baerends, E. J.; Ellis, D. E.; Ros, P. *Chem. Phys.* **1973**, *2*, 41–51.
(30) Fonseca Guerra, C.; Visser, O.; Snijders, J. G.; te Velde, G.; Baerends, E. J. *Methods and Techniques for Computational Chemistry*; STEF: Cagliari, Italy, 1995.
(31) te Velde, G.; Bickelhaupt, F. M.; Baerends, E. J.; Fonseca Guerra, C.; van Gisbergen, S. J. A.; Snijders, J. G.; Ziegler, T. *J. Comput. Chem.* **2001**, *22*, 931.
(32) Ravenek, W. In *Algorithms and applications on vector and parallel computers*; te Riele, H. J. J., Dekker, T. J., van de Vorst, H. A., Eds.; Elsevier: Amsterdam, The Netherlands, 1987.
(33) te Velde, G.; Baerends, E. J. *J. Comput. Phys.* **1992**, *99*, 84–98.
(34) Snijders, J. G.; Baerends, E. J.; Vernooijs, P. *At. Nucl. Data Tables* **1982**, *26*, 483–509.
(35) Vernooijs, P.; Snijders, J. G.; Baerends, E. J. *Slater Type Basis Functions for the Whole Periodic System*; Internal Report; Vrije Universiteit: Amsterdam, The Netherlands, 1981.
(36) Krijn, J.; Baerends, E. J. *Fit Functions in the HFS Method*; Internal Report (in Dutch); Vrije Universiteit: Amsterdam, The Netherlands, 1984.

(37) Slater, J. C. *Quantum Theory of Molecules and Solids*; McGraw-Hill: New York, 1974; Vol. 4.
(38) Vosko, S. H.; Wilk, L.; Nusair, M. *Can. J. Phys.* **1980**, *58*, 1200–1211.
(39) Versluis, L.; Ziegler, T. *J. Chem. Phys.* **1988**, *28*, 322–328.
(40) Becke, A. D. *Phys. Rev. A* **1988**, *38*, 3098–3100.
(41) Perdew, J. P. *Phys. Rev. B* **1986**, *33*, 8822–8824.
(42) ADF 2000; Vrije Universiteit: Amsterdam, The Netherlands, 2000.
(43) Parr, R. G.; von Szentpaly, L.; Liu, S. *J. Am. Chem. Soc.* **1999**, *121*, 1922–1924.
(44) Geerlings, P.; De Proft, F.; Langenaeker, W. *Chem. Rev.* **2003**, *103*, 1793–1873.
(45) Parr, R. G.; Yang, W. *Density Functional Theory of Atoms and Molecules*; Oxford University Press: New York, 1989.
(46) Parr, R. G.; Donnelly, R. A.; Levy, M.; Palke, W. E. *J. Chem. Phys.* **1978**, *68*, 3801–3807.
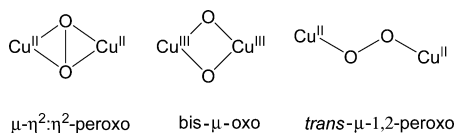(47) Parr, R. G.; Pearson, R. G. *J. Am. Chem. Soc.* **1983**, *105*, 7512–7516.
(48) Koopmans, T. *Physica* **1934**, *1*, 104–113.
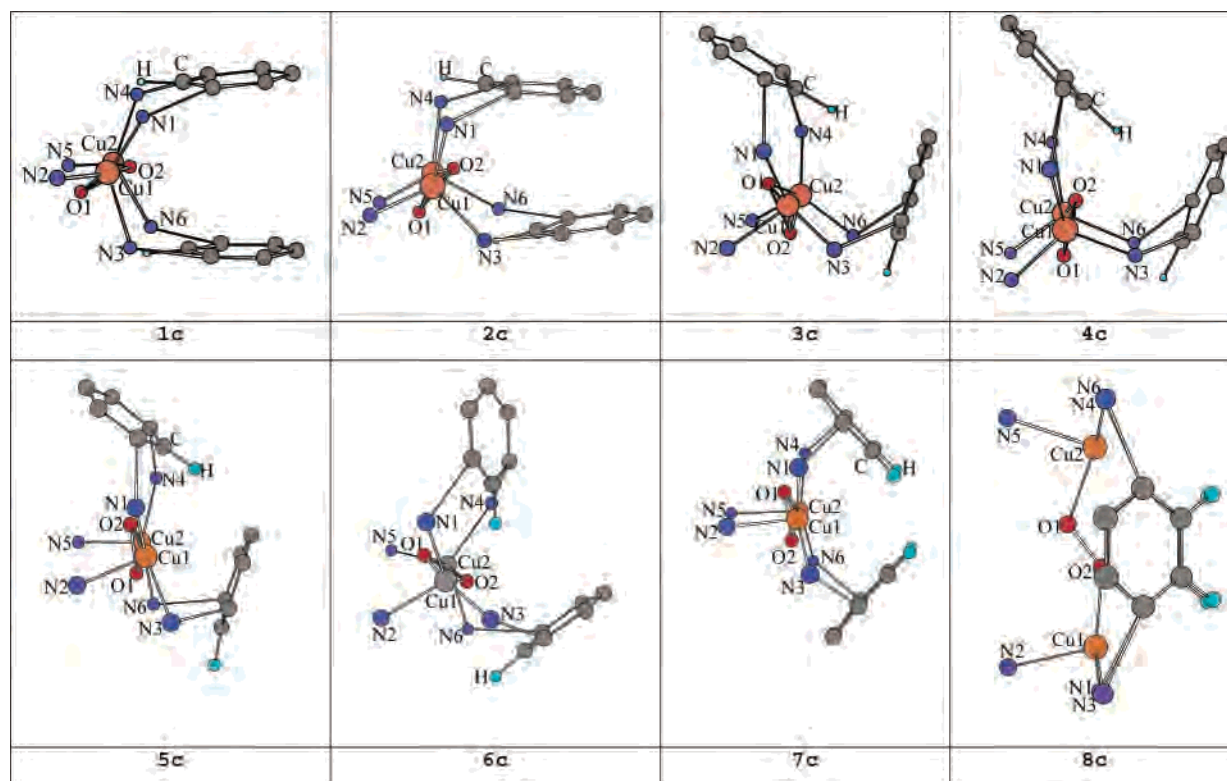
Figure 1. Calculated structures for μ-η^2:η^2-peroxo side-on complexes **1c**−**7c** and *trans-μ*-1,2-peroxo **8c**. The methylenic units linking amines or phenyl units as well as H atoms have been omitted for clarity.

Chart 2. Cu_2O_2 Core Structures Discussed in the Present Work

Results

Singlet vs Triplet State. The optimized structures obtained for the peroxo $Cu^{II}_2(\mu$-$O_2)$ complexes **1c**−**8c** are depicted in Figure 1. All attempts to optimize $Cu^{III}_2(\mu$-$O)_2$ complexes starting from **3c** and **4c** by increasing the O−O distance have reverted to the peroxo species (see Chart 2 for a drawing of the core structures).

Optimizations were carried out for the charged 2+ closed-shell singlet ground-state structures, except for **8c**, for which the triplet state is the ground state. For **1c**−**7c**, the energy difference between singlet and triplet states ranges from 0.7 kcal·mol^{-1} for the peroxo species **3c** and **4c** to 11.2 kcal·mol^{-1} for **5c**. We have also performed spin-unrestricted broken-symmetry calculations for the singlet diradical state. Starting from unsymmetrical wave functions, we have observed in all cases reconvergence to the restricted solution. This means that, at least at the present BP86//VWN level of theory, the restricted singlet is the ground state. It has been shown by different authors[49−53] that delocalized states are

overstabilized with present pure density functionals as a result of a bad cancellation of the self-interaction included in the coulombic energy by the exchange-correlation functional. As a result, closed-shell singlet states are energetically favored by DFT with respect to open-shell diradical singlet states, although in some cases, the open-shell diradical singlet states are still found to be the most stable.[54] This overstabilization of delocalized states is partially corrected when using hybrid functionals, especially those that incorporate a large percentage of exact Hartree−Fock exchange.[54] For this reason, we have further analyzed the relative stability of the restricted closed-shell and diradical singlets with the hybrid functionals B3LYP[55−57] and BHLYP[58] at the VWN-optimized geometries using *Gaussian03*[59] and the 6-31G** basis set.[60] Convergence to the open-shell diradical singlet state for our systems was not achieved, and in all cases, spin-unrestricted broken-symmetry calculations reverted to the restricted solution. Thus, the present results clearly favor the closed-shell singlet state as the ground state of complexes **1c**−**7c**.

It is worth noting that **8c**, which contains the Me2p ligand, represents a special case as far as the ground-state multiplicity is concerned. For this compound, a *trans-μ*-1,2-peroxo structure with the Cu atoms separated by 4.7 Å was

(49) Braïda, B.; Hiberty, P. C.; Savin, A. *J. Phys. Chem. A* **1998**, *102*, 7872−7877.
(50) Sodupe, M.; Bertran, J.; Rodríguez-Santiago, L.; Baerends, E. J. *J. Phys. Chem. A* **1999**, *103*, 166−170.
(51) Chermette, H.; Ciofini, I.; Mariotti, F.; Daul, C. *J. Chem. Phys.* **2001**, *115*, 11068−11079.
(52) Grüning, M.; Gritsenko, O. V.; van Gisbergen, S. J. A.; Baerends, E. J. *J. Phys. Chem. A* **2001**, 9211−9218.
(53) Poater, J.; Solà, M.; Rimola, A.; Rodríguez-Santiago, L.; Sodupe, M. *J. Chem. Phys. A* **2004**, 6072−6078.
(54) Metz, M.; Solomon, E. I. *J. Am. Chem. Soc.* **2001**, *123*, 4938−4950.
(55) Becke, A. D. *J. Chem. Phys.* **1993**, *98*, 5648−5652.
(56) Lee, C.; Yang, W.; Parr, R. G. *Phys. Rev. B* **1988**, *37*, 785−789.
(57) Stephens, P. J.; Devlin, F. J.; Chabalowski, C. F.; Frisch, M. J. *J. Phys. Chem.* **1994**, *98*, 11623−11627.
(58) Becke, A. D. *J. Chem. Phys.* **1993**, 1372−1377.

Table 1. Selected Metric Parameters for Calculated Structures **1c−8c**

interm. species	d(Cu1−Cu2)	d(O1−O2)	d(Cu1−O1)	d(Cu1−O2)	d(Cu2−O1)	d(Cu2−O2)	d(Cu1−N)	d(Cu2−N)	d(O−C) (d(O−H))[a]	dihedral angle Cu1−O1−O2−Cu2
							1.972	2.997		
							2.016	1.994	2.553	
1c	3.595	1.414	2.034	1.867	2.050	1.864	2.097	2.085	(2.202)	167.8
							1.956	1.980		
							1.996	1.967	2.346	
2c	3.568	1.429	2.008	1.886	1.998	1.879	2.118	2.158	(2.364)	164.7
							2.012	2.015		
							2.219	2.025	2.643	
3c	3.455	1.435	1.910	1.942	1.912	1.931	2.024	2.015	(2.626)	150.9
							2.017	2.004		
							1.994	2.009	2.522	
4c	3.605	1.429	1.984	1.910	2.009	1.897	2.174	2.168	(2.041)	169.2
							2.092	2.015		
							2.290	2.177	2.452	
5c	3.582	1.418	1.951	1.969	1.922	1.953	2.103	2.182	(2.468)	161.3
							2.169	2.191		
							2.013	2.098	2.578	
6c	3.738	1.412	1.946	2.033	2.115	1.904	2.119	2.021	(2.800)	175.1
							2.047	2.043		
							2.219	2.215	2.959	
7c	3.574	1.420	1.951	1.946	1.943	1.956	2.036	2.034	(3.519)	159.9
							2.074	2.112		
							2.099	2.166	2.724	
8c	4.677	1.301	2.938	1.878	1.922	2.840	2.123	2.107	(2.800)	162.5

[a] These values correspond to the distance between the O1 or O2 oxygen atoms, from the Cu_2O_2 core to the closest aromatic C−H bond of the macrocyclic ligand.

optimized (see Figure 1). This is probably due to the presence of the methyl groups and the para substitution in the aromatic linkers of Me2p, which force the Cu atoms to be particularly distant. In its optimized ground-state geometry, the rhombic structure of the $Cu^{II}_2(\mu\text{-}\eta^2\text{:}\eta^2\text{-}O_2)$ core is lost, resulting in a complex that is more stable in the triplet state rather than in the singlet state. Consequently, this complex has the same multiplicity as the free O_2 molecule and to a large extent retains its molecular character. This is corroborated by the short distance between O atoms (1.301 Å), which is significantly shorter than that in **7c**. It should be mentioned here that experimentally characterized *trans-μ*-1,2-peroxo-dicopper(II) complexes described so far in the literature are diamagnetic (singlet state).[61] However, one has to take into account that in **8c** the much longer Cu···Cu distance and the much shorter O−O bond length (4.677 and 1.301 Å, respectively) as compared to the structurally characterized *trans-μ*-1,2-peroxodicopper(II) complex described by Karlin et al. (4.359 and 1.432 Å, respectively)[61] favor the triplet state.

Structures of Calculated Peroxo Complexes. Complexes **1c−7c** exhibit a distorted $Cu^{II}_2(\mu\text{-}\eta^2\text{:}\eta^2\text{-}O_2)$ core where the Cu centers adopt a highly distorted square-pyramidal geometry, as depicted in Figure 1. Selected metric parameters for structures **1c−8c** are displayed in Table 1.

Complexes **3c**, **5c**, and **7c** adopt a square-pyramidal geometry where the central N atoms occupy the apical positions. The same structure is found for complexes **1c**, **2c**, and **4c**, but in these cases, the apical positions are occupied by the benzylic N atoms of one of the arene rings. Complex **6c** possesses a completely different arrangement: one of the Cu centers has a benzylic N atom in the apical position, whereas in the other one, it is occupied by the central N atom. Cu ions in **8c** display a distorted tetrahedral geometry.

Complexes **1c** and **2c**, containing the Schiff base ligands sb2m and sb3m, adopt a relatively similar global conformation where the aromatic rings are placed nearly parallel (the dihedral angles between the planes defined by the two aromatic rings are 4.4° and 13.4°, respectively). This suggests that the geometry imposed by the imine bonds is a key factor influencing the overall geometry of the complex, whereas the number of methylenic groups linking the amine−imine N atoms exerts only a fine-tuning effect on the relative disposition of the Cu_2O_2 core with regard to the aromatic rings. In this situation, the closest O···C$_{ar}$ and O···H$_{ar}$ distances (O atom from the peroxo core and H and C atoms from the closest C−H group of the aromatic rings) for complexes **1c** and **2c** are relatively similar (see Table 1).

Complexes **3c** and **4c**, which contain meta-substituted secondary amine ligands, share a similar geometry that is

(59) Frisch, M. J.; Trucks, G. W.; Schlegel, H. B.; Scuseria, G. E.; Robb, M. A.; Cheeseman, J. R.; Montgomery, J. A.; Vreven, T.; Kudin, K. N.; Burant, J. C.; Millam, J. M.; Iyengar, S. S.; Tomasi, J.; Barone, V.; Mennucci, B.; Cossi, M.; Scalmani, G.; Rega, N.; Petersson, G. A.; Nakatsuji, H.; Hada, M.; Ehara, M.; Toyota, K.; Fukuda, R.; Hasegawa, J.; Ishida, M.; Nakajima, T.; Honda, Y.; Kitao, O.; Nakai, H.; Klene, M.; Li, X.; Knox, J. E.; Hratchian, H. P.; Cross, J. B.; Adamo, C.; Jaramillo, J.; Gomperts, R.; Stratmann, R. E.; Yazyev, O.; Austin, A. J.; Cammi, R.; Pomelli, C.; Ochterski, J. W.; Ayala, P. Y.; Morokuma, K.; Voth, G. A.; Salvador, P.; Dannenberg, J. J.; Zakrzewski, V. G.; Dapprich, S.; Daniels, A. D.; Strain, M. C.; Farkas, Ö.; Malick, D. K.; Rabuck, A. D.; Raghavachari, K.; Foresman, J. B.; Ortiz, J. V.; Cui, Q.; Baboul, A. G.; Clifford, S.; Cioslowski, J.; Stefanov, B. B.; Liu, G.; Liashenko, A.; Piskorz, P.; Komaromi, I.; Martin, R. L.; Fox, D. J.; Keith, T.; Al-Laham, M. A.; Peng, C. Y.; Nanayakkara, A.; Challacombe, M.; Gill, P. M. W.; Johnson, B.; Chen, W.; Wong, M. W.; Gonzalez, C.; Pople, J. A. *Gaussian03*; Gaussian, Inc.: Pittsburgh, PA, 2003.
(60) Frisch, M. J.; Pople, J. A.; Binkley, J. S. *J. Chem. Phys.* **1984**, *80*, 3265−3269.
(61) Tyeklár, Z.; Jacobson, R. R.; Wei, N.; Murthy, N. N.; Zubieta, J.; Karlin, K. D. *J. Am. Chem. Soc.* **1993**, *115*, 2677−2689.

Table 2. Decomposition Energy Analysis (kcal·mol^{-1}) of the BE of O$_2$ in Cu$^{II}_2$ (μ-η^2:η^2-O$_2$) Intermediate Species

intermediate species	$\Delta E_{\text{def O}_2}$	$\Delta E_{\text{def complex}}$	ΔE_{def}	ΔE_{int}	BE
1c	16.5	12.8	29.3	−48.8	−19.7
2c	18.9	12.7	31.7	−51.3	−19.6
3c	19.8	28.2	48.0	−67.1	−19.1
4c	18.9	28.6	47.6	−61.5	−13.9
5c	17.3	22.4	39.7	−48.5	−8.8
6c	16.3	24.3	40.6	−52.2	−11.6
7c	17.5	42.9	60.4	−62.9	−2.5

completely different from that of the previous cases. Now the aromatic rings are placed nearly perpendicular to each other, and the number of methylenic units between secondary amines strongly influences the relative orientation of the Cu$_2$O$_2$ core. The O···C$_{ar}$ and O···H$_{ar}$ distances are particularly short for complex **4c**.

The geometry adopted by complex **5c** is similar to its secondary amine analogue **3c**, and thus the potential geometric distortion exerted by the encumbrance of the six methyl groups of the tertiary amines is nearly negligible. In sharp contrast, the structure of complex **6c** is strongly influenced by the steric effects produced by the six methyl groups. A view along the Cu···Cu axis reveals that the six N-methyl groups are situated in an octahedral-like alternate manner. In these two cases, the O···C$_{ar}$ and O···H$_{ar}$ distances are relatively large.

Complex **7c**, substituted in the para position, presents a global conformation relatively similar to its meta isomer **3c**. However, the para substitution of the aromatic ring generates a relative disposition of its aromatic C−H bonds that end up much further away from the O core atoms than those in the previous cases.

BEs and Electrophilic Character of the Cu$_2$O$_2$ Core. The energies released when molecular O$_2$ binds to the binuclear macrocycles to form the μ-η^2:η^2-peroxo species are given in Table 2. This energy decreases in the order **1c** > **2c** > **3c** > **4c** > **6c** > **5c** > **7c**. In general, when the basic character of the macrocyclic ligand increases, the absolute value of the BE is reduced. Thus, there is a slight diminution when going from the complex **1c** bearing the sb2m Schiff base ligand to the **3c** bearing the H2m ligand. There is also a decrease when going from the secondary amine ligands to the corresponding tertiary amine ones (compare **3c** with **5c** and **4c** with **6c**). Finally, we also found a reduction in the BE when a methylenic group is added to the aliphatic chain of the macrocycle (compare complexes bearing ligands sb2m with sb3m and H2m with H3m), with the exception of **5c** and **6c** containing tertiary amine ligands. These results can be understood from the correlation diagram that describes the orbitals most involved in the bonding between the Cu dimer and the O$_2$ molecule depicted in Figure 2. As can be seen, the key interaction is the one involving the (d$_{xy}$)$_1$ + (d$_{xy}$)$_2$ orbital of the Cu dimer with the π_x* orbital of the O$_2$ molecule. One can expect that the smaller the energy difference between these two orbitals, the larger the interaction energy. When the basicity of the macrocycle increases, the energy of the (d$_{xy}$)$_1$ + (d$_{xy}$)$_2$ orbital of the Cu dimer rises and consequently the energy released in the
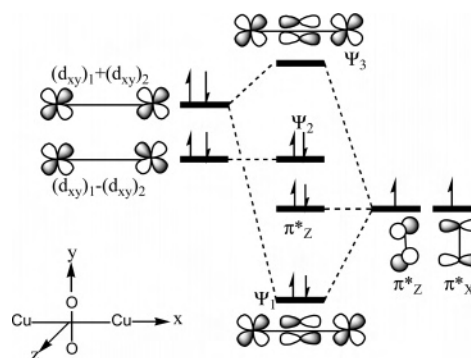
Figure 2. Correlation diagram that describes the main orbitals involved in the bonding between the Cu dimer and O$_2$ molecule in the ground state.

interaction between the Cu dimer and the O$_2$ molecule decreases. Factors such as the Cu···Cu distance may also have an important effect. Indeed, an increase of the Cu···Cu distance should stabilize the (d$_{xy}$)$_1$ + (d$_{xy}$)$_2$ orbital of the Cu dimer and produce an increase of the absolute value of the BE. However, this effect is partially compensated for by a reduction of the overlap between the (d$_{xy}$)$_1$ + (d$_{xy}$)$_2$ orbital of the Cu dimer and the π_x* orbital of the O$_2$ molecule. The low (in absolute value) energy associated with O$_2$ binding in **7c** (containing the H2p ligand) as compared to **3c** (containing the H2m ligand) is related to the larger deformation energy needed to modify the geometry of the [Cu$_2$(H2p)]$^{2+}$ complex to reach the structure that this fragment has in the μ-η^2:η^2-peroxo form (vide infra).

To gain a deeper insight into its nature, we have split up the BEs of all μ-η^2:η^2-peroxo species into a deformation energy term (ΔE_{def}) and an interaction energy term (ΔE_{int}). The results are gathered in Table 2. The ΔE_{def} total values range from 29.3 kcal·mol^{-1} (**1c**) to 60.4 kcal·mol^{-1} (**7c**). The deformation energy of the O$_2$ molecule is almost constant for all complexes (from 16.3 to 19.8 kcal·mol^{-1}), being somewhat larger for **3c** (19.8 kcal·mol^{-1}), which is the complex with the most activated O−O bond and largest O−O bond length. The large ΔE_{def} of complex **7c** is due to the large structural changes that the Cu$^I_2$ should undergo to form the final oxygenated structure. This is clearly reflected in the shortening of the Cu···Cu distance from 6.172 to 3.574 Å when the Cu$_2$O$_2$ intermediate **7c** species is formed. Interestingly, the complexes bearing more rigid ligands undergo less deformation in their original structures and thus lead to lower deformation energies and, in general, more negative BEs. The ΔE_{int} terms take values from −48.5 kcal·mol^{-1} (**5c**) to −67.1 kcal·mol^{-1} (**3c**).

The electrophilicity of these peroxo compounds was calculated using the parameter defined by Parr and co-workers[43] (see eq 1). Table 3 contains the energies of the HOMO (ϵ_H) and LUMO (ϵ_L) and the μ, η, and ω values obtained from eqs 1−3 by using the frontier orbital energies (ϵ_H and ϵ_L). It is important to notice that the electrophilicity value is especially low for complex **2c**, as compared to that of complex **1c**. The main difference comes from the hardness value; i.e., the HOMO−LUMO gap is larger for the **2c** case. The electrophilicity of intermediate species **8c** has not been included because of its open-shell nature, which makes the

Table 3. HOMO and LUMO Energies, Chemical Potential, Hardness, and Electrophilicity for the Different Complexes Analyzed Together with Mulliken Charges of Cu and O Atoms[a]

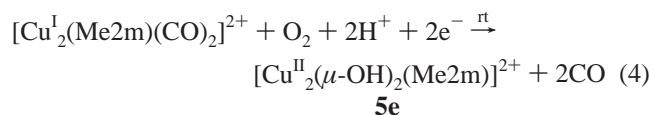| intermediate species	ϵ_{HOMO}	ϵ_{LUMO}	μ	η	ω	$q_{Cu1+Cu2}$	q_{O1+O2}
1c	−247.5	−229.5	238.5	9.0	3163.1	1.647	−0.993
2c	−250.1	−226.1	238.1	12.0	2364.5	1.546	−1.017
3c	−243.4	−225.3	234.4	9.1	3033.7	1.607	−1.018
4c	−242.6	−222.2	232.4	10.2	2648.4	1.456	−1.016
5c	−243.2	−226.5	234.8	8.3	3309.5	1.772	−0.963
6c	−241.1	−223.9	232.5	8.6	3138.5	1.745	−0.956
7c	−243.8	−227.2	235.5	8.3	3330.9	1.547	−0.962

[a] Units for energies, chemical potential, hardness, and electrophilicity are kcal·mol^{-1} and electrons for charges.

calculation of the hardness and chemical potential more difficult and their comparison with closed-shell species not feasible. Nevertheless, this structure has nucleophilic character according to Hatcher and Karlin.[62]

Finally, in Table 3, we have also collected the Mulliken charge distribution for the Cu_2O_2 core. Qualitatively, the results are the same using the Hirshfeld or Voronoi charges. The charges on the C and H atoms of the C−H bonds with a high probability of being attacked are very similar. The main differences are observed in the charges of the O and Cu atoms for the different complexes. Interestingly, complexes showing larger electrophilicities are also those that have less negative O atoms.

Synthesis and Structure of Oxidized Complexes. Binuclear copper(II) hydroxide complexes with ligands H3m, Me2m, and Me2p were prepared from the corresponding colorless copper(I) carbonyl complexes (which are easily generated from their respective Cu^I complexes by bubbling CO into the solution)[22] upon oxidation with molecular O_2 at room temperature. Carbonyl complexes were employed because of their improved stability in relation to their corresponding nitrile analogues.

For the Me2m ligand, the final product obtained is a blue-green binuclear bis(μ-hydroxy)copper(II) complex, **5e**.

$$[Cu^I_2(Me2m)(CO)_2]^{2+} + O_2 + 2H^+ + 2e^- \xrightarrow{rt}$$
$$[Cu^{II}_2(\mu\text{-}OH)_2(Me2m)]^{2+} + 2CO \quad (4)$$
$$\textbf{5e}$$

Instead, for the Cu$^I_2$ complex with the isomeric Me2p ligand, the product obtained upon oxygenation is also a binuclear bis(hydroxy)copper(II) complex, $[Cu^{II}(OH)_2(Me2p)]^{2+}$ (**8e**), but with the hydroxide ligands binding in the terminal mode.

Alternatively, compounds **5e** and **8e** could be directly prepared by the reaction in acetonitrile of the respective macrocyclic ligand (Me2m or Me2p), $Cu(CF_3SO_3)_2$, and NaOH in molar ratio 1:2:2.

Finally, the oxygenation of the binuclear Cu^I complex containing the H3m ligand leads to intramolecular O_2 atom insertion into the phenyl ring, generating a binuclear Cu^{II} complex with both phenolate and hydroxide bridges, $[Cu^{II}\text{-}(H3m\text{-}O)(\mu\text{-}OH)]^{2+}$ (**4e**), where H3m-O represents the deprotonated/oxygenated H3m ligand. This new heptadentate macrocycle was obtained as a free ligand, H3m-OH, by treating **4e** with aqueous ammonia and extracting it with dichloromethane.

The oxygenation of binuclear Cu^I complexes with the ligands sb2m and sb3m was previously studied by Menif and Martell and Schindler et al.[24,25] These studies revealed that only the Cu$_2$ complex containing the sb2m ligand undergoes arene hydroxylation upon reaction with O_2. However, the exact nature of the Cu^{II} macrocyclic complexes formed upon O_2 reaction could not be established by crystallography. Comba et al. have also demonstrated that the Cu$_2$ complex containing the sb2p ligand does not react with O_2.[63]

The crystal structures of complexes **4e**, **5e**, and **8e** have been determined by means of single-crystal X-ray diffraction analysis. Table 4 contains crystallographic data for complexes **4e**, **5e**, and **8e**, whereas Table 5 contains selected bond distances and angles. ORTEP diagrams of the cationic molecular structures of complexes **4e**, **5e**, and **8e** are displayed in Figure 3.

The cationic part of **5e** consists of the macrocyclic ligand Me2m binding two Cu atoms and two hydroxide molecules acting in a bridging mode. The molecule has a C2 axis that runs through the bridging O atoms. Each Cu atom possesses a distorted square-pyramidal geometry with a τ factor of 0.23.[64] The two bridging hydroxide ligands and two N atoms from the macrocyclic ligand (N2 and N3) occupy the base of the pyramid, forming a five-membered chelate ring, whereas the apical position is occupied by N1 ($d_{Cu-N1} = 3.02$ Å, indicating only a slight contact). The two pyramids are relatively arranged so that they share a basal edge, constituted by the two bridging O atoms, with the apical vertexes pointing out in opposite directions.

The cationic part of **8e** consists of the macrocyclic ligand (Me2p), binding two Cu atoms and with two OH ligands acting in a terminal mode. The Cu atoms have a distorted square-planar geometry with the benzylic amine atoms N1A and N3B slightly off the plane. Bond distances are within the values measured for related compounds.[65−70] The CuA−O1A and CuB−O1B bond distances are 1.857(5) and 1.846(5) Å, respectively, which are close to the values described in the literature for terminal Cu^{II}−OH bonds.[71−76]

(62) Hatcher, L. Q.; Karlin, K. D. *J. Biol. Inorg. Chem.* **2004**, *9*, 669−683.

(63) Comba, P.; Hambley, T. W.; Hilfenhaus, P.; Richens, D. T. *J. Chem. Soc., Dalton Trans.* **1996**, *4*, 533−539.

(64) Addison, A. W.; Rao, T. N.; Reedijk, J.; Van Rijn, J.; Verschoor, G. C. *J. Chem. Soc., Dalton Trans.* **1984**, *7*, 1349−1346.

(65) Becker, M.; Heinemann, F. W.; Knoch, F.; Donaubauer, W.; Liehr, G.; Schindler, S.; Golub, G.; Cohen, H.; Meyerstein, D. *Eur. J. Inorg. Chem.* **2000**, *4*, 719−726.

(66) Becker, M.; Heinemann, F. W.; Schindler, S. *Chem.−Eur. J.* **1999**, *5*, 3124.

(67) Barlow, S. J.; Hill, S. J.; Hocking, J. E.; Hubberstey, P.; Li, W.-S. *J. Chem. Soc., Dalton Trans.* **1997**, *24*, 4701−4704.

(68) Bazzicalupi, C.; Bencini, A.; Bianchi, A.; Fusi, V.; Giorgi, C.; Paoletti, P.; Stefani, A.; Valtancoli, B. *Inorg. Chem.* **1995**, *34*, 552−559.

(69) Scott, M. J.; Lee, S. C.; Holm, R. H. *Inorg. Chem.* **1994**, *33*, 4651−4662.

(70) Bailey, N. A.; Fenton, D. E.; Gonzalez, M. S. L. *Inorg. Chim. Acta* **1984**, *88*, 125−134.

(71) Arii, H.; Funahashi, Y.; Jitsukawa, K.; Masuda, H. *J. Chem. Soc., Dalton Trans.* **2003**, *11*, 2115−2116.

(72) Harata, M.; Jitsukawa, K.; Masuda, H.; Einaga, H. *Bull. Chem. Soc. Jpn.* **1998**, *71*, 637−645.

Table 4. Crystallographic Data for **4e**(PF$_6$)$_2$·0.5CH$_3$CN, **5e**(ClO$_4$)$_2$·2CH$_3$OH, and **8e**(CF$_3$SO$_3$)$_2$·5H$_2$O

compound	**4e**(PF$_6$)$_2$·0.5CH$_3$CN	**5e**(ClO$_4$)$_2$·2CH$_3$OH	**8e**(CF$_3$SO$_3$)$_2$·5H$_2$O
cryst size [mm]	0.45 × 0.20 × 0.10	0.50 × 0.25 × 0.15	0.13 × 0.13 × 0.09
empirical formula	C$_{30}$H$_{49}$Cu$_2$F$_{12}$N$_7$O$_2$P$_2$	C$_{32}$H$_{52}$Cl$_2$Cu$_2$N$_6$O$_{12}$	C$_{32}$H$_{62}$Cu$_2$F$_6$N$_6$O$_{13}$S$_2$
M_r	956.78	910.78	1044.08
T [K]	298(2)	298(2)	100(2)
cryst syst	orthorhombic	monoclinic	triclinic
space group	$Pna2(1)$	$C2/c$	$P\bar{1}$
a [Å]	22.107(6)	14.685(4)	11.0621(8)
b [Å]	18.991(3)	17.307(4)	14.3804(10)
c [Å]	9.440(2)	16.475(3)	15.9531(12)
α [deg]	90	90	64.451(2)
β [deg]	90	93.30 (2)	75.017(2)
γ [deg]	90	90	77.383(2)
V [Å^3]	3962.9(15)	4180.2(2)	2195.1(3)
Z	4	4	2
ρ_{calcd} [g·cm^{-3}]	1.604	1.447	1.580
μ [mm^{-1}]	1.249	1.208	1.155
λ [Å]	0.710 73	0.710 73	0.71073
$F(000)$	1960	1896	1088
θ range [deg]	1.41−27.55	1.82−25.04	1.44−25.05
h, k, l collected	−28 ≤ h ≤ 27	−17 ≤ h ≤ 8	−13 ≤ h ≤ 13
	−23 ≤ k ≤ 24	−20 ≤ k ≤ 20	−17 ≤ k ≤ 15
	−11 ≤ l ≤ 12	−18 ≤ l ≤ 19	−18 ≤ l ≤ 13
no. of reflns measd	8887	8684	12176
no. of unique reflns	6755	3679	7661
param/restraints	569/76	241/1	633/0
GOF^a (all data)	1.137	1.036	0.875
final R^a indices [$I > 2\sigma(I)$]	R1 = 0.0541, wR2 = 0.1258	R1 = 0.0647, wR2 = 0.1807	R1 = 0.0651, wR2 = 0.1411
R^a indices (all data)	R1 = 0.0803, wR2 = 0.1435	R1 = 0.0918, wR2 = 0.2060	R1 = 0.1350, wR2 = 0.1637
$\Delta\rho$ (max/min) [e·Å^{-3}]	−0.327/0.454	−0.731/1.053	−0.489/1.158

^{a} R1 = $\sum ||F_o| - |F_c||/\sum|F_o|$ and wR2 = $(\sum[w(F_o^2 - F_c^2)^2]/\sum[wF_o^4])^{1/2}$, where $w = q/\sigma^2(F_o^2) + (aP)^2 + bP$.

Table 5. Selected Bond Lengths (Å) and Angles (deg) for **4e**(PF$_6$)$_2$·0.5CH$_3$CN, **5e**(ClO$_4$)$_2$·2CH$_3$OH, and **8e**(CF$_3$SO$_3$)$_2$·5H$_2$O

4e(PF$_6$)$_2$·0.5CH$_3$CN		**5e**(ClO$_4$)$_2$·CH$_3$CN		**8e**(CF$_3$SO$_3$)$_2$·5H$_2$O	
Cu1−O2	1.918(4)	Cu1−O1	1.922(4)	CuA−O1A	1.857(5)
Cu1−N1	1.981(5)	Cu1−O2	1.935(4)	CuA−N2A	1.998(6)
Cu1−O1	2.033(4)	Cu1−N2	2.014(4)	CuA−N3A	2.074(5)
Cu1−N2	2.053(4)	Cu1−N3	2.054(4)	CuA−N1A	2.080(5)
Cu1−N3	2.320(6)	Cu1−Cu12	3.0110(14)	CuB−O1B	1.846(5)
Cu2−O2	1.920(4)	O1−Cu1−O2	77.3(2)	CuB−N2B	1.995(6)
Cu2−N6	1.969(5)	O1−Cu1−N2	99.38(19)	CuB−N3B	2.084(6)
Cu2−O1	2.022(3)	O2−Cu1−N2	174.67(16)	CuB−N1B	2.089(6)
Cu2−N5	2.058(4)	O1−Cu1−N3	160.62(14)	CuA−CuB	6.7143(13)
Cu2−N4	2.340(5)	O2−Cu1−N3	97.71(18)	O1A−CuA−N2A	176.8(2)
Cu1−Cu2	3.0457(9)	N2−Cu1−N3	86.74(19)	O1A−CuA−N3A	94.0(2)
O2−Cu1−N1	165.6(2)			N2A−CuA−N3A	84.2(2)
O2−Cu1−O1	77.12(14)			O1A−CuA−N1A	97.8(2)
N1−Cu1−O1	92.9(2)			N2A−CuA−N1A	84.7(2)
O2−Cu1−N2	92.7(2)			N3A−CuA−N1A	160.1(2)
N1−Cu1−N2	91.6(2)			O1B−CuB−N2B	176.7(2)
O1−Cu1−N2	152.2(2)			O1B−CuB−N3B	97.1(2)
O2−Cu1−N3	93.4(2)			N2B−CuB−N3B	85.1(2)
N1−Cu1−N3	100.2(2)			O1B−CuB−N1B	94.3(3)
O1−Cu1−N3	114.6(2)			N2B−CuB−N1B	84.4(3)
N2−Cu1−N3	91.5(3)			N3B−CuB−N1B	159.7(2)
O2−Cu2−N6	167.5(2)				
O2−Cu2−O1	77.34(14)				
N6−Cu2−O1	93.9(2)				
O2−Cu2−N5	92.2(2)				
N6−Cu2−N5	91.7(2)				
O1−Cu2−N5	152.8(2)				
O2−Cu2−N4	91.9(2)				
N6−Cu2−N4	99.8(2)				
O1−Cu2−N4	113.0(2)				
N5−Cu2−N4	92.1(2)				

The O atom of the terminal hydroxide group is weakly intramolecularly H-bound to six H atoms (H1BB, H9BB, H2BB, H8BC, H14A, and H15B) and intermolecularly bound by a strong H bond to another Cu−OH group, O1A_2 from

(73) Allen, W. E.; Sorrell, T. N. *Inorg. Chem.* **1997**, *36*, 1732−1734.
(74) Berreau, L. M.; Mahapatra, S.; Halfen, J. A.; Young, V. G., Jr.; Tolman, W. B. *Inorg. Chem.* **1996**, *35*, 6339−6342.
(75) Fusch, G.; Fusch, E. C.; Erxleben, A.; Hüttermann, J.; Scholl, H.-J.; Lippert, B. *Inorg. Chim. Acta* **1996**, *252*, 167−178.
(76) Lee, S. C.; Holm, R. H. *J. Am. Chem. Soc.* **1993**, *115*, 11789−11798.
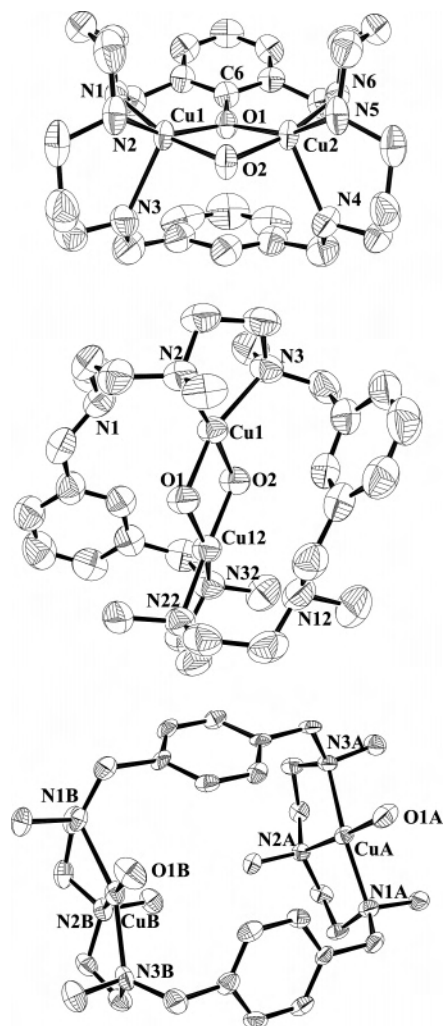
Figure 3. ORTEP diagram of the cationic portion of **4e** (top), **5e** (middle), and **8e** (bottom).

a symmetry-related molecule (D−H; O1A−H1A/O1B−H1B, d(D−H); 0.840/0.840, d(H···A); 2.164/2.214, ∠DHA; 145.54/138.34, d(D···A); 2.896/2.896). Figure 4 shows the dimer-of-dimer complex generated by these intermolecular H bonds.

The structure of **4e** consists of the macrocyclic ligand acting as a heptadentate ligand (H3m-O). Six amino groups are bound to the two Cu atoms together with a bridging hydroxide ligand and a bridging phenolate coming from the macrocyclic ligand. The molecule has a pseudo plane of symmetry that bisects the two aromatic rings and contains the two O bridging atoms. The geometry of the Cu atoms is best described by a slightly distorted square-planar pyramid with $\tau = 0.24$[64] and with the bases of both pyramids sharing one edge (O1 and O2 atoms). The bases of the pyramids are not coplanar and show a hinge angle of 139.42°, leading to a roof-shape core for Cu_2O_2.

Spectroscopic and Magnetic Properties of the Oxidized Complexes. The most prominent UV−vis spectral features of complexes **4e**, **5e**, and **8e** are described in the Experimental Section. These complexes show bands in the 600−700 nm region with low extinction coefficients, typically expected for d−d types of transitions,[77] and bands below 400 nm due

to hydroxide (phenolate)-to-Cu^{II} charge-transfer and $\pi-\pi^*$ transitions of the ligands.

Figure 5 presents a graph of the molar χ_M^*T product vs T for compounds **4e** and **5e**. For **5e**, at 298 K the value of χ_M^*T is 0.446 cm³·K·mol⁻¹ and decreases continuously until 140 K, where it levels off, manifesting a strong antiferromagnetic (AF) coupling between the two Cu^{II} metal centers. A similar trend is also observed for complex **4e** but with lower χ_M^*T values and with the curvature change taking place at about 180 K (see Figure 5), which is indicative of an even stronger AF coupling. In contrast, for complex **8e**, the χ_M^*T value at 298 K is 0.686 cm³·K·mol⁻¹, and it slightly increases until a maximum value of 0.69 cm³·K·mol⁻¹ at 100 K (see the Supporting Information). Then χ_M^*T slightly decreases until 10 K, where it suddenly drops, giving a value of χ_M^*T equal to 0.52 cm³·K·mol⁻¹ at 2 K. This is the typical magnetic behavior of uncoupled Cu^{II} ions, thus manifesting the inability of the two metal centers in complex **8e** to magnetically communicate, through space, through the macrocyclic ligand backbone, or through H bonds. The X-band EPR spectrum of **8e** at 20 K in frozen CH_3OH consists of a nearly axial signal, best simulated as $g_x = 2.02$, $g_y = 2.05$, $g_z = 2.3$, $A_{xx} = 40$, $A_{yy} = 60$, and $A_{zz} = 90$ G, characteristic of a $d_{x^2-y^2}$ ground state. Double integration against a $[Cu^{II}(EDTA)]$ standard provides two spin units (±10%) per complex, confirming that the two Cu centers are independent spin units.

For complexes **4e** and **5e**, the heights of the plateau at low temperatures are indicative of the presence of Curie-behaved impurities. Thus, the equations used to fit the experimental data include the term ρ and are based on the Hamiltonian.

$$H = -JS_1S_2 + \beta HgS$$

$$\chi_M T = (Ng^2\beta^2/k)[2 \exp(J/kT)/(1 + 3 \exp(J/kT)](1 - \rho) + (Ng^2\beta^2/2k)\rho$$

Using these equations, the values that best fit the curves are as follows: **5e**, $J = -286.3$ cm⁻¹, $g = 2.07$, $\rho = 0.064$, $R = 2.6 \times 10^{-3}$; **4e**, $J = -482.0$ cm⁻¹, $g = 2.30$, $\rho = 0.032$, $R = 5.6 \times 10^{-3}$. The contribution of the temperature-independent paramagnetism was shown to have no significant effect in these cases and thus is not included in the calculations.

Discussion

Theoretical Prediction of the Influence of the Macrocyclic Ligand on the Formation of the Cu_2O_2 Cores and Their Evolution. Previous work by Karlin, Tolman, Stack, and others has shown that using different bidentate or tridentate alkylamine ligands and depending on the solvent, and/or counteranions, a given Cu^I complex interacts with molecular O_2 to form $\mu\text{-}\eta^2{:}\eta^2$-peroxo- and/or bis-$\mu$-oxodicopper complexes and that these species might be in rapid equilibrium.[78−80] In a recent work, Karlin and co-workers,[81]

(77) Hathaway, B. J.; Billing, D. E. *Coord. Chem. Rev.* **1970**, *5*, 143−207.
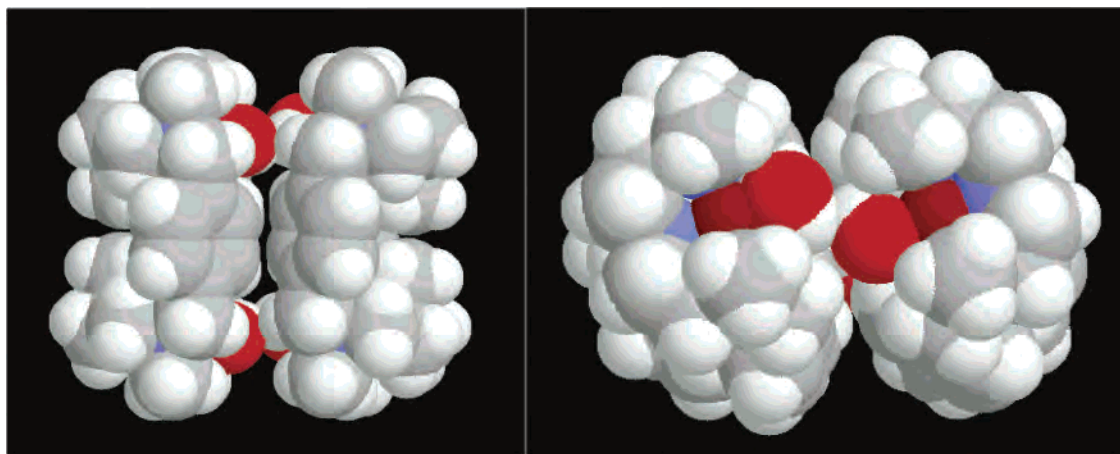
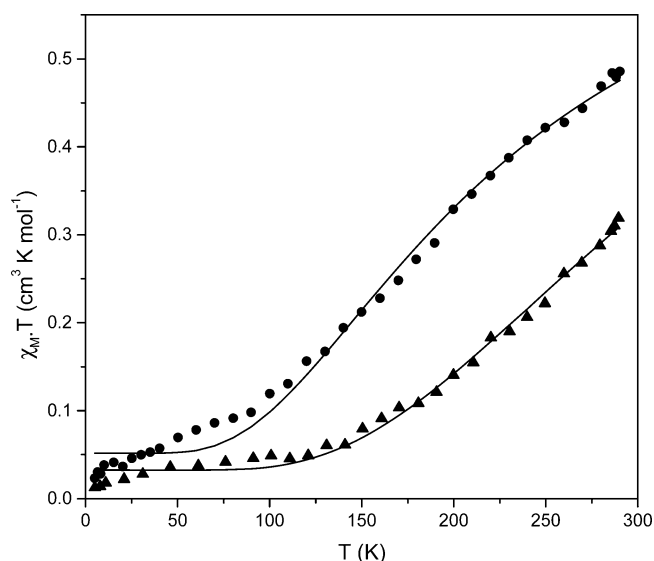**Figure 4.** Compact view of the dimer-of-dimer formation in complex **8e**, through Cu−OH hydrogen bonds.

Figure 5. $\chi_M T$ vs T experimental data for **4e** (▲) and **5e** (●) (cm³·K·mol⁻¹). The solid line shows the best fit obtained (see the text).

using simple alkyltriamine types of ligands, have illustrated once more the delicate equilibrium between the isomeric forms of the Cu_2O_2 core structures by simply changing a coordinating secondary amine by a tertiary amine. In the present work, no peroxo- or bis-μ-oxodicopper species bearing the macrocyclic ligands displayed in Chart 1 have been experimentally detected, even at low temperatures. However, theoretical calculations have revealed that in our case the side-on peroxo isomer is likely to be the only possible isomer because no optimized structures for the bis-μ-oxo isomers of **3c** and **4c** were located.

Complexes **1c**−**7c** possess a μ-η^2:η^2-peroxodicopper(II) core and exhibit larger O−O distances than the free O_2 molecule in its ground state (1.218 Å at the VWN/DZP level

of theory), as well as a shorter Cu⋯Cu distance than the initial unreacted Cu_2 complexes. Interestingly, there is a strong correlation between the O−O bond length and the Cu⋯Cu distance [$d(O-O) = -0.1114d(Cu-Cu) + 1.8222$, and $R^2 = 0.9794$] for complexes **1c**−**7c** (Table 1).

For the series of macrocyclic complexes displayed in Chart 1, the aromatic substitution in the meta or para position strongly influences the nature of the intermediate species formed. Complex **7c** (containing the H2p ligand) has the lowest BE (Table 2) mainly because of the unfavorable contribution of a large ΔE_{def} factor. This is a consequence of the relative disposition of the Cu centers imposed by the para substitution, together with the increase of the internal macrocyclic ring by two units (which by definition is the largest cycle that contains the metal centers in the initial Cu complex), with regard to its meta isomer (**3c**). In complex **8c** (which contains the Me2p ligand), there is a further increase in the steric crowding compared to **7c** because of the methyl groups of the tertiary amines. This causes the instability of the *side-on* peroxo species, and now only the *end-on* peroxo isomer is obtained, thus providing an example of how steric factors can control the nature of the reactive intermediate species.

For complexes **1c**−**6c** (that contain a meta-substituted ligand), the number of methylenic units as well as the nature of the linking N atoms strongly influences the electronic properties of the peroxo core, as can be seen in Tables 2 and 3. The ligands also influence the spatial arrangement of the Cu_2O_2 core with regard to the phenyl ring, which is also a key factor that determines the performance of these complexes especially from an intramolecular viewpoint.

There is experimental evidence that only complexes **1c** and **4c** bearing the sb2m[24,25,82,83] and H3m (this work) ligands possess reactive species that lead toward the intramolecular hydroxylation of an aromatic C−H bond, a reaction that has been shown to take place via a nucleophilic attack of the aromatic ring toward the electrophilic *side-on* peroxo Cu_2O_2 core.

(78) Stack, T. D. P. *J. Chem. Soc., Dalton Trans.* **2003**, *10*, 1881−1889.
(79) Henson, M. J.; Mukherjee, P.; Root, D. E.; Stack, T. D. P.; Solomon, E. I. *J. Am. Chem. Soc.* **1999**, *121*, 10332−10345.
(80) (a) Halfen, J. A.; Mahapatra, S.; Wilkinson, E. C.; Kaderli, S.; Young, V. G., Jr.; Que, L., Jr.; Zuberbühler, A. D.; Tolman, W. B. *Science* **1996**, *271*, 1397−1400. (b) Tolman, W. B. *Acc. Chem. Res.* **1997**, *30*, 227−237.
(81) Liang, H.-C.; Zhang, C. X.; Henson, M. J.; Sommer, R. D.; Hatwell, K. R.; Kaderli, S.; Zuberbühler, A. D.; Rheingold, A. L.; Solomon, E. I.; Karlin, K. D. *J. Am. Chem. Soc.* **2002**, *124*, 4170−4171.

(82) Menif, R.; Martell, A. E.; Squattrito, P. J.; Clearfield, A. *Inorg. Chem.* **1990**, *29*, 4723−4729.
(83) Ma, H.; Allmendinger, M.; Thewalt, U.; Lentz, A.; Klinga, M.; Rieger, B. *Eur. J. Inorg. Chem.* **2002**, 2857−2867.

It is worth noting that complexes **1c** and **4c** are among the ones having the smallest distances between the C—H$_{arom}$ group and one of the two O atoms. Thus, a possible rule of reactivity, only based on geometric factors, is that a system will be reactive if the sum of the two shortest O···H and O···C distances in the μ-η^2:η^2-peroxo form is smaller than 4.75 Å. This requirement is only accomplished by **1c**, **2c**, and **4c**, and except for **2c**, it fully coincides with the experimental evidence.

However, as shown in Table 3, complex **2c** has by far the lowest electrophilicity (mainly because of a large hardness value; the HOMO—LUMO gap), which prevents its Cu$_2$O$_2$ core from undergoing an aromatic nucleophilic attack. Thus, it constitutes an example of how the electronic factors transmitted by the macrocyclic ligand predominate over the geometric factors also established by these ligands. In addition, we can briefly mention that the orientation of the aromatic rings in **4c** suggests that hydroxylation occurs through a σ^* mechanism according to the classification by Decker et al.[84]

Complex **6c** possesses a unique structure in this family of complexes in the sense that each Cu center has two different types of apical coordinating N atoms and that the relative disposition of the six N atoms is octahedral instead of trigonal-prismatic. Thus, a comparison of the structures of **4c** and **6c** reveals how the steric effect of the six methyl groups can strongly influence the geometry of the complex.

Influence of the Macrocyclic Ligand on the Nature of the Evolved Cu Complexes. Single-crystal X-ray diffraction analysis of complex **8e** showed two hydroxide groups coordinated in a monodentate terminal mode and a relative syn disposition. This molecular arrangement is very similar to that of [Cu$_2$Cl$_2$(Me2p)$_2$]$^{2+}$ except that the Cl atoms have been replaced by hydroxide ligands.[85] To the best of our knowledge, **8e** constitutes the first example of a binuclear Cu^{II} complex containing two terminal OH ligands. Although dinuclear bis(μ-hydroxy)copper(II) complexes are very common, Cu compounds containing terminally bound hydroxide ligands are rare because of their tendency to bridge. Indeed, this is a general trend for first-row late-transition-metal complexes containing this type of ligand. Isolation of M—OH (M = Mn, Fe, Co, Ni, Cu, or Zn) types of species usually requires stabilization of the unit by H-bonding and/or protection by steric groups.[86]

In the particular case of **8e**, the stabilization of the terminal Cu—OH unit is achieved by the steric encumbrance of the macrocyclic ligand, which does not allow the formation of intramolecular Cu$^{II}_2$(μ-OH)$_2$ bridges, and by a number of H bonds. Each terminal Cu—OH group has six medium-to-weak intramolecular H bonds (see Figure 4) and a relatively strong intermolecular H bond with another symmetry-related molecule that generates the dimer-of-dimer complex shown in Figure 4.

In sharp contrast, in **5e** the arene rings are meta-substituted, which causes a shrinking of the internal cavity by two member units. As a consequence, the geometry of the macrocycle allows the formation of the highly stable bis(μ-hydroxy) binuclear complex. However, the topology of the Me2m ligand still does not have a perfect fit for the metal center, and thus its rigidity is responsible for the distortion of the local Cu geometry. In turn, this geometrical distortion influences the capacity of the metal centers to magnetically couple, as will be discussed in the following section.

Complex **4e** constitutes a completely different example of evolution of the O oxidative equivalents leading to intramolecular arene hydroxylation. This reaction mimics tyrosinase's activity, and thus **4a** constitutes a monooxygenase functional model.[12,17] While this type of insertion is now well documented in model complexes,[19] the structure of **4e** is unique in the sense that the constraints imposed by the macrocyclic ligand are responsible for the hinge distortion of the Cu$_2$O$_2$ core that results in a roof-shape core.

Influence of the Macrocyclic Ligand on the Magnetic Properties Displayed by the Cu$_2$ Complexes 4e, 5e, and 8e. In complex **8e**, the geometry of the Me2p ligand does not allow the formation of either phenolate or hydroxide bridging ligands; as a consequence, there is no efficient magnetic coupling between metal centers, and therefore it behaves as a typical uncoupled Curie magnet. The square-pyramidal coordination geometry around each Cu metal center is manifested in the electron spin resonance parameters where $g_z = 2.20 > g_y = 2.05 \sim g_x = 2.05$.

From a magnetic viewpoint, complexes **4e** and **5e** belong to the broad and largely studied family of binuclear Cu^{II} complexes doubly bridged by O ligands. Several magneto-structural correlations and theoretical studies have been carried out[87-100] for these types of compounds, where it is

(84) Decker, H.; Dillinger, R.; Tuczek, F. *Angew. Chem., Int. Ed.* **2000**, *39*, 1591−1595.
(85) Bazzicalupi, C.; Bencini, A.; Bianchi, A.; Fusi, V.; Giorgi, C.; Paoletti, P.; Stefani, A.; Valtancoli, B. *Inorg. Chem.* **1995**, *34*, 552−559.
(86) MacBeth, C. E.; Hammes, B. S.; Young, V. G., Jr.; Borovik, A. S. *Inorg. Chem.* **2001**, *40*, 4733−4741.

(87) Crawford, V. H.; Richardson, H. W.; Wasson, J. R.; Hodgson, D. J.; Hatfield, W. E. *Inorg. Chem.* **1976**, *15*, 2107−2110.
(88) Hodgson, D. J. *Prog. Inorg. Chem.* **1975**, *19*, 173−241.
(89) Handa, M.; Koga, N.; Kida, S. *Bull. Chem. Soc. Jpn.* **1988**, *61*, 3853−3857.
(90) Nieminen, K. *Ann. Acad. Sci. Fennicae A II* **1982**, *197*, 1−60.
(91) Walz, L.; Paulus, H.; Haase, W. *J. Chem. Soc., Dalton Trans.* **1985**, 913−920.
(92) Bencini, A.; Gatteschi, D. *Inorg. Chim. Acta* **1978**, *31*, 11−18.
(93) Hay, P. J.; Thibault, J. C.; Hoffman, R. *J. Am. Chem. Soc.* **1975**, *97*, 4884−4889.
(94) Kahn, O. *Inorg. Chim. Acta* **1982**, *62*, 3−14.
(95) Coomarmond, J.; Plumere, P.; Lehn, J. M.; Agnus, Y.; Louis, P.; Weiss, R.; Kahn, O.; Morgenstern-Badarau, I. *J. Am. Chem. Soc.* **1982**, *104*, 6330−6340.
(96) Astheimer, H.; Haase, W. *J. Chem. Phys.* **1986**, *85*, 1427−1432.
(97) Ruiz, E.; Alemany, P.; Alvarez, S.; Cano, J. *J. Am. Chem. Soc.* **1997**, *119*, 1297−1303.
(98) Ruiz, E.; Alemany, P.; Alvarez, S.; Cano, J. *Inorg. Chem.* **1997**, *36*, 3683−3688.
(99) Blanchet-Boiteux, C.; Muesca, J. M. *J. Phys. Chem. A* **2000**, *104*, 2091−2097.
(100) Merz, L.; Haase, W. *J. Chem. Soc., Dalton Trans.* **1980**, 875−879.
(101) Torelli, S.; Belle, C.; Gautier-Luneau, I.; Pierre, J. L.; Saint-Aman, E.; Latour, J. M.; Pape, L. L.; Luneau, D. *Inorg. Chem.* **2000**, *39*, 3526−3536.
(102) Nishida, Y.; Shimo, H.; Marea, H.; Kida, S. *J. Chem. Soc., Dalton Trans.* **1985**, 1945−1950.
(103) Bertoncello, K.; Fallon, G. D.; Hodgkin, J. H.; Murray, K. S. *Inorg. Chem.* **1988**, *27*, 4750−4758.
(104) Fallon, G. D.; Murray, K. S.; Spethmann, B.; Yandell, J. K.; Hodgkin, J. H.; Loft, B. C. *J. Chem. Soc., Chem. Commun.* **1984**, 1561−1563.

Table 6. Magnetostructural Parameters for Five-Coordinated Complexes Containing a $Cu^{II}(\mu\text{-OPh})(\mu\text{-OH})Cu^{II}$ Core

complex[a]	Cu−O$_H$−Cu (deg)	Cu−O$_{Ph}$−Cu (deg)	Cu−O−Cu mean value (deg)	J^b (cm^{-1})	geometry type[c]	ref
[Cu$_2$(L^{14})(OH)](ClO$_4$)$_2$	102.1	95.7	98.9	−224	tbp	101
[Cu$_2$(L^{13})(OH)](ClO$_4$)$_2$	104.8	99.1	101.9	−675	tbp	102
[Cu$_2$(H3m-O)(OH)](ClO$_4$)$_2$ (**4e**)	105.0	97.4	101.2	−482	sp	c
[Cu$_2$(L^4)(OH)](ClO$_4$)$_2$	99.2	104.1	101.6	∼0	sp	83
[Cu$_2$(L^5)(OH)(H$_2$O)$_2$](ClO$_4$)$_2$	96.5	91.5	94.0	∼0	sp	103, 104
[Cu$_2$(L^7)(OH)(ClO$_4$)](ClO$_4$)	100.4	99.2	99.8	−364	sp	105
[Cu$_2$(L^3)(OH)](BF$_4$)$_2$	103.6	101.9	102.7	−420	sp	110
[Cu$_2$(L^1)(OH)](PF$_6$)$_2$	104.4	102.5	103.4	−600	sp	106, 107
[Cu$_2$(L^{11})(OH)(ClO$_4$)$_2$]	106.5	96.9	101.7	−809	sp	108

[a] Ligands L^x are 2,6-R-phenolate derivatives, with different R substituents; L^{14} = 2,6-bis[[bis(2-pyridylmethyl)amino)methyl]-4-methylphenolate, L^{13} = 2,6-bis{bis[2-(methylthio)ethyl]aminomethyl}-4-methylphenolate; L^4 = p-tBu-sb2m-O; L^5 = 2,6-bis[(N-methylpiperazino)methyl[-4-chlorophenolate, L^7 = 2,6-bis[N-(2-pyridylmethyl)formidoyl]-4-methylphenolate, L^3 = 2,6-bis{{bis[2-(1-pyrazolyl)ethyl]amino}methyl}-p-cresolato, L^1 = bis{[bis-2(pyridyl)ethyl]amine}-m-xylenolato, L^{11} = 2,6-bis[4-(2-benzimidazolyl)-2-thiabutyl]-4-methylphenolate. [b] J values are based on Hamiltonian $H = -JS_1S_2$; tbp = trigonal bipyramidal and sp = square pyramidal. [c] This work.

shown that the major factor influencing the exchange is the angle of the Cu−O−Cu bridge (α). However, there are other significant factors that may contribute to the increase of the ferromagnetic character and that can effectively reduce any AF term generally associated with the bridges; those factors include structural distortions and the ligand basicity.

Compounds **5e** and **4e** show an important AF coupling, which is larger for the mixed (μ-hydroxo)(μ-phenoxo) bridging ligand, **4e**, than for the bis(μ-hydroxy), **5e**. The Cu−O−Cu average angle is quite similar for both compounds (101.2° for **4e** and 102.7° for **5e**). For compound **5e**, with two hydroxide bridging ligands, the expected J value from the empirical correlation reported by Hatfield et al.[87] would be −384 cm^{-1}, which is much larger than what we find, −286 cm^{-1}. The decrease in the predicted AF character could be due to the structural distortion of the Cu$_2$O$_2$ core imposed by the Me2m ligand as well as the deviation of the bound N atoms from the plane defined by the Cu$_2$O$_2$ core. Another factor that can also produce a certain decrease of the AF character is the basicity of the amines.[97,98]

Table 6 summarizes the five-coordinated complexes with a (μ-phenoxo)(μ-hydroxo) type of core reported in the literature together with some structural parameters. As can be observed, there is no clear-cut relationship between the Cu−O−Cu angles and the magnetic coupling constant for all of the complexes. The J value obtained for **4e** is only 482 cm^{-1}. Probably this is because of geometrical factors imposed by the nature of the macrocyclic ligand, which have been previously described to lower the AF character: (a) the hinged nature of the Cu$_2$O$_2$ core and (b) the bending of the OH and OC bonds with regard to the O- - -O axis.

A more detailed description of the magnetic properties is provided in the Supporting Information.

Conclusion

DFT calculations for binuclear Cu complexes (**1c−8c**), containing the macrocyclic ligands shown in Chart 1 and the Cu$_2$O$_2$ core, have proven to be an excellent tool to envisage reactive intermediate species that cannot be experimentally detected and characterized. Furthermore, these DFT calculations have also provided an excellent guide to unravel their potential reactivity based on the relative disposition of the aromatic rings and the Cu$_2$O$_2$ core and also on their electronic properties (mainly their electrophilicity). This has allowed rationalization of the nature of the evolved oxidized species based on the nature of the macrocyclic ligand, a fact that could not have been understood otherwise. Three evolved complexes **4e**, **5e**, and **8e** have been obtained by different routes and structurally, spectroscopically, and magnetically characterized. Even though they contain relatively similar macrocyclic dinucleating ligands, complexes **4e**, **5e**, and **8e** present radically different structures and magnetic properties. Thus, they constitute an example of how subtle ligand variations, in binuclear complexes bearing dinucleating ligands, can strongly influence chemical and physical behavior.

Supporting Information Available: Cartesian *xyz* atomic coordinates for all of the calculated optimized geometries, crystallographic information files (CIF) for **4e**, **5e**, and **8e**, and additional spectral and magnetic data. This material is available free of charge via the Internet at http://pubs.acs.org.

IC051800J

(105) O'Connor, C. J.; Firmin, D.; Pant, A. K.; Babu, B. R.; Stevens, E. D. *Inorg. Chem.* **1986**, *25*, 2300−2307.
(106) Karlin, K. D.; Farooq, A.; Hayes, J. C.; Cohen, B. I.; Rowe, T. M.; Sinn, E.; Zubieta, J. *Inorg. Chem.* **1987**, *26*, 1271−1280.
(107) Karlin, K. D.; Hayes, J. C.; Gultneh, Y.; Cruse, R. W.; McKown, J. W.; Hutchinson, J. P.; Zubieta, J. *J. Am. Chem. Soc.* **1984**, *106*, 2121−2128.
(108) Benzekri, A.; Dubourdeaux, P.; Latour, J.-M.; Laugier, J.; Rey, P. *Inorg. Chem.* **1988**, *27*, 3710−3716.